Location-Specific Prediction of the Probability of Occurrence and Quantity of Precipitation over the Western Himalayas

U. C. MOHANTY AND A. P. DIMRI

Centre for Atmospheric Sciences, Indian Institute of Technology, Delhi, India

(Manuscript received 11 February 2003, in final form 19 November 2003)

ABSTRACT

Northwest India is composed, in part, of complex Himalayan mountain ranges having different altitudes and orientations, causing the prevailing weather conditions to be complex. During winter, a large amount of precipitation is received in this region due to eastward-moving low pressure synoptic weather systems called western disturbances (WDs). The objective of the present study is to use the perfect prognostic method (PPM) for probability of precipitation (PoP) forecasting and quantitative precipitation forecasting (QPF). Three observatories in the western Himalayan region, namely, Sonamarg, Haddan Taj, and Manali, are selected for development of statistical dynamical models for location-specific prediction of the occurrence and quantity of precipitation. Reanalysis data from the National Centers for Environmental Prediction (NCEP), and upper-air and surface observations from the India Meteorological Department (IMD), are used to develop statistical dynamical models for PoP and QPF for winter, that is, December, January, February, and March (DJFM). Models are developed with data from DJFM 1984–96 and tested with data from DJFM 1996–97. Four experiments are carried out with four different sets of predictors to evaluate the performance of the models with independent datasets. They are 1) NCEP–NCAR reanalysis data, 2) operational analyses from the National Centre for Medium Range Weather Forecasting (NCMRWF) in India, 3) day 1 forecasts with a T80 global spectral model at NCMRWF, and 4) forecasts from the regional fifth-generation Pennsylvania State University–NCAR Mesoscale Model (MM5) day 1 forecast. Forecast skills are examined for these four experiments and for direct numerical model outputs of T80 day 1 and MM5 day 1 forecasts at these three stations. It is found that a best prediction is made with an accuracy of 89% at Haddan Taj using the MM5 day 1 forecast as predictors in the PoP model. In the case of the QPF model, a maximum 85% accuracy is achieved using the MM5 day 1 forecast variables as predictors. Thus, use of numerical model output from MM5 as predictors in statistical dynamical models based on the PPM concept provides definite improvements in the prediction of occurrence and quantity of precipitation as compared to the direct numerical model output.

1. Introduction

The western Himalayas and adjoining Indian region receive a high amount of precipitation during the winter season, mainly in the form of snow. This precipitation severely affects human activities due to cold wave conditions and avalanches. Winter precipitation is mainly attributed to the passage of weather systems called western disturbances (WDs). These are eastward-moving low pressure synoptic weather systems that originate over the Mediterranean Sea or mid–Atlantic Ocean and travel eastward over Iran, Afghanistan, Pakistan, and northwest India. These weather systems take their southernmost tracks during winter and pass over northwest India. These WDs yield large amounts of precipitation during winter months, namely, December, January, February, and March (DJFM), in the form of snow. Sometimes the WDs also come from eastward-moving extratropical cyclones penetrating far southward. Northwest India has complex mountain ranges. Surface weather elements like precipitation and temperature are highly dependent upon local topography and local atmospheric circulations. It is very difficult to simulate/predict such surface weather elements over complex mountainous region by even sophisticated state-of-the-art numerical weather prediction (NWP) models. Precipitation is one of the important weather elements that influence various activities. Statistical relations are developed between precipitation at the location of interest and nearby observed values of surface and upper-air weather elements by using carefully chosen predictors and suitable statistical techniques. Two prominent methods for producing statistical-based forecasts are the perfect prognostic method (PPM) of Klein et al. (1959) and the model output statistics (MOS) approach of Glahn and Lowry (1972). Probability of precipitation (PoP) and quantitative precipitation forecasting (QPF) at a specific site and time can provide important guidance for human

Corresponding author address: Prof. U. C. Mohanty, Centre for Atmospheric Sciences, Indian Institute of Technology, Hauz Khas, New Delhi-110016, India.
E-mail: mohanty@cas.iitd.ernet.in

activity, preparations for natural hazards (such as avalanches and floods), and forest management.

Various statistical techniques are available for predicting PoP and QPF. Glahn and Lowry (1969, 1972) used outputs from NWP models to develop regression models to forecast PoPs over different parts of the United States. Paegle (1974) compared the forecast of PoPs over different parts of the United States derived from equations stratified with respect to the synoptic weather patterns and equations that were not stratified. It was found that the stratified methods were more accurate. Kriplani and Singh (1986) developed composite charts of probabilities of 24-h rainfall amounts exceeding 2.5 and 65 mm, when a monsoon depression is over India. Upadhyay et al. (1986) developed a method to forecast precipitation by considering the fact that the precipitation rates are directly proportional to the large-scale vertical velocity. Using this method, precipitation rates were computed for specific monsoon depression situations over central parts of India. Kruizinga (1982) compared the forecasting of PoPs over the Netherlands using an analog technique and logistic regression. At 1–3-day lead time, the regression method performed better than the analog technique. Carter et al. (1989) discussed the performance of statistical forecasts that are routinely issued by the U.S. National Weather Service for the contiguous United States and Alaska. Kumar and Ram (1995) developed a technique for quantitative precipitation forecasting over the Rapti catchment region in Uttar Pradesh, India. This is a synoptic-analog method in which synoptic systems are classified according to the observed rainfall rates in the ranges 11–25, 26–50, and $>$50 mm. Mohanty et al. (2001) developed objective methods to forecast PoP and QPF at Delhi using classical multivariate regression and discriminant analysis. Maini et al. (2002) employed the perfect prognostic method for precipitation and temperature forecasts during the monsoon season.

Thus, the use of objective techniques to forecast precipitation for a specific location in the mountainous region of northwest India is limited. None of these studies dealt with mountainous regions such as northwest India. It may be noted that in mountainous regions mainly synoptic, persistence, climatological methods are used to predict the occurrence of precipitation. Forecasts based on persistence show very poor results, as precipitation has a strong temporal and spatial variability over the region. Further, over the mountainous region, the meso-/microscale circulation plays an important role in determining the amount of precipitation. In recent years with the establishment of the National Centre for Medium Range Weather Forecasting (NCMRWF) in New Delhi, a direct numerical model output operationally provides precipitation forecasts over the western Himalayas with a horizontal model resolution of 1.5° latitude $\times$ 1.5° longitude. The performance of NWP models over this region is severely constrained due to complex topography as well as a lack of adequate observations. Further, the surface heterogeneity of northwest India generates numerous meso-/microscale circulations in the narrow valleys and rugged hills, which dominate in determining the precipitation patterns in the region. In view of this, large-scale general circulation models with coarse horizontal resolution can not properly simulate the quantity of precipitation and its horizontal distribution.

Therefore, there is a need for more skillful objective methods to predict precipitation over mountains. It is also desirable to introduce statistical–dynamical modeling to downscale the numerical model outputs using either the PPM or MOS method to produce PoP and QPF guidance over the region. Developing statistical–dynamical models for PoP and QPF is a difficult task over rugged mountainous regions like the western Himalayas. This is mainly due to the highly heterogeneous terrain and the nonavailability of adequate observational datasets. The authors are unaware of any study on PoP and QPF models for the western Himalayas and adjoining mountainous region of northwest India. Thus, the prediction of the occurrence–nonoccurrence of precipitation is a challenging task over the western Himalayas.

In the present study, the PPM concept is preferred over MOS because MOS requires a large sample of numerical model output with a specific model. MOS does not have flexibility with respect to the use of many different models (such as a global circulation model, regional model, and/or mesoscale model). In the region under consideration NWP models are still under refinement as better computing facilities and observations from the western Himalayas become available. On the other hand the PPM approach is quite flexible as it is developed based on past observations/analyses. The performance of the PPM with independent datasets will depend upon the quality of the NWP output. Any refinement in the specific numerical model does not require redevelopment of the PPM model, which is not the case with MOS.

The goal of the paper is to develop a statistical–dynamical model for PoP and QPF over the western Himalayas using the PPM concept. The data source, quality control, and data preparation for the model development are presented in section 2. Section 3 describes the development of the PoP forecast model. QPF model formulation is presented in section 4. Section 5 describes the experiments carried out to evaluate the performance of the PoP and QPF models. In section 6 the results and discussion are presented. Finally section 7 contains the broad conclusions of the study.

2. Data and analysis procedure

The precipitation distribution over the western Himalayas is very complex. Daily precipitation for the region 26.25°–38.75°N 66.25°–78.75°E is derived at 2.5° $\times$ 2.5° latitude–longitude grid points for the period

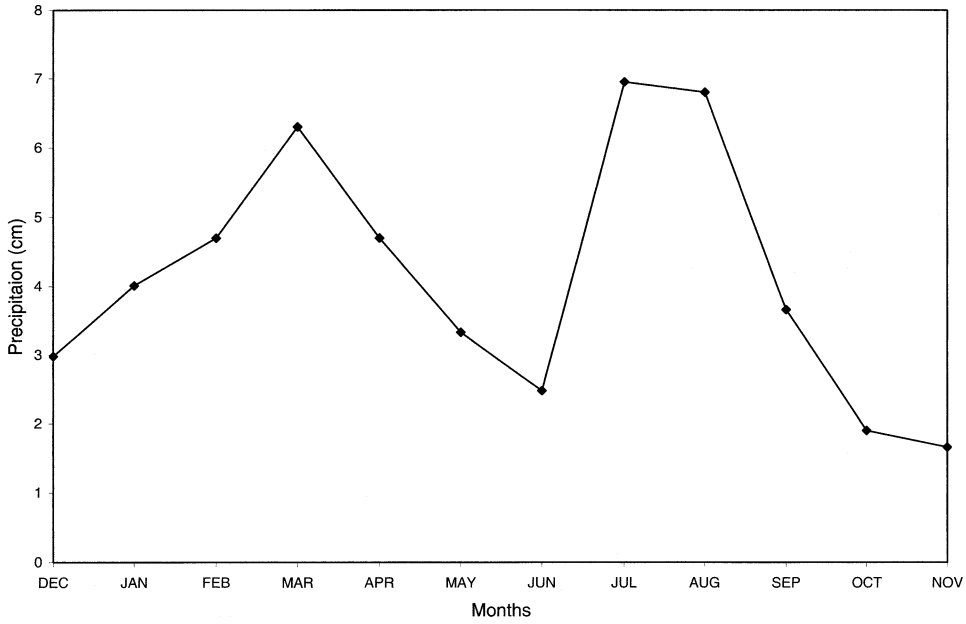

FIG. 1. Averaged monthly precipitation (cm of liquid water equivalent) over the region of interest (26.25°–38.75°N, 66.25°–78.75°E) in the western Himalayas.

1958–97 from the National Centers for Environmental Prediction–National Center for Atmospheric Research (NCEP–NCAR) reanalysis dataset and monthly averages are computed. The area-average monthly precipitation plot is shown in Fig. 1. The precipitation distribution shows two maxima. The primary maximum occurs in summer (July–August), whereas the secondary maximum occurs in March. Generally, winter precipitation occurs in the form of snow over the hilly ranges and glacier basins and accumulates throughout the winter season to feed the river systems during the summer.

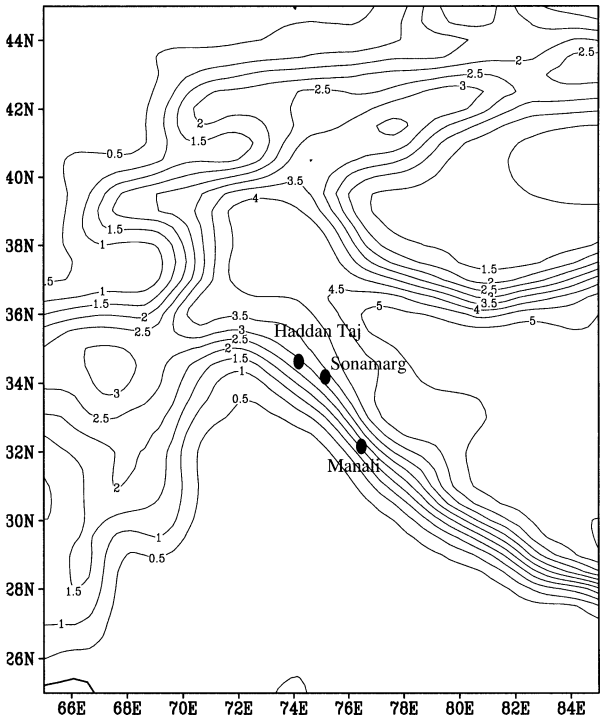

FIG. 2. Locations selected for the study and contoured topography (*10^3 m).

For the development of the PoP and QPF models, three locations are selected in the western Himalayan region of Jammu and Kashmir, and Himachal Pradesh: Sonamarg (latitude 34°18′11″N, longitude 75°17′57″E, and altitude 2745 m), Haddan Taj (latitude 34°18′43″N, longitude 74°02′42″E, and altitude 3080 m), and Manali (latitude 32°19′27″N, longitude 77°13′27″E, and altitude 2192 m) (see Fig. 2). Long and continuous past datasets are available at these sites, so they are convenient for the development of PoP and QPF models. These three sites represent three distinct climatic zones of the western Himalayas. Haddan Taj is situated at the northwest part of the Pir Panjal range, while Manali is situated in the northeast part of the same range. Sonamarg is situated between them in the Great Himalayan range. These three locations show different climatic characteristics and their geographical locations and situations give rise to different local mesoscale weather systems. Out of these stations, Sonamarg and Manali are situated on a national highway and provide avalanche warnings for remote areas. Wintertime precipitation, in the form of snow, gives rise to numerous avalanches along the road. The climatology of mean monthly snowfall amount and temperature for winter months is presented in Table 1. Large amounts of precipitation pose a threat to lives and property in snowbound regions. Similarly, falling temperatures brings

TABLE 1. Climatological distribution of average monthly snowfall (cm of snow depth) and mean monthly dry-bulb temperature (°C).

	Avg monthly snowfall (cm)			Mean monthly dry-bulb temp (°C)		
Month	Sonamarg	Haddan Taj	Manali	Sonamarg	Haddan Taj	Manali
Dec	210	162	44	−2.1	−1.6	7.0
Jan	186	173	108	−4.2	−2.8	4.6
Feb	255	244	109	−4.3	−4.4	5.7
Mar	351	229	90	−1.6	−1.0	8.7

cold wind conditions in conjunction with eastward-moving synoptic weather systems.

At least 5–6 yr of data are required for the development of statistical models (Carter 1986). Due to the complex geographical situation of the Himalayas, 12 yr are used here for developing stable statistical–dynamical models for PoP and QPF. The model equations are developed using surface and upper-air data for DJFM for the 12-yr period 1984–96. The models are then tested with independent datasets for DJFM for the period 1996–97. Upper-air and surface observations at and around the selected locations are considered, so that advection effects can be taken into account. As an adequate number of surface and upper-air stations are not available in and around the data-sparse western Himalayas, long-period large-scale global analyses of meteorological fields such as the NCEP–NCAR reanalysis (Kalnay et al. 1996) are also used.

Before selecting potential predictors, care was taken to carry out quality control of observational data and to fill data gaps. In order to detect and correct errors, the mean ($\overline{x}$) and standard deviation (σ) of all the parameters were calculated. All observations of individual parameters that lie outside ($\overline{x} \pm 3\sigma$) were isolated and examined. After examining previous and subsequent meteorological observations and synoptic weather conditions, outliers were replaced by suitable values. Once the errors were identified and corrected, the next step was to identify the missing data and fill the data gaps using suitable interpolations. The individual data gaps were filled using linear interpolation. Observations at nearby observatories were also given some consideration, while filling the individual data gaps. By doing so, quality control checks and consistency checks on the space, time, and synoptic condition were made.

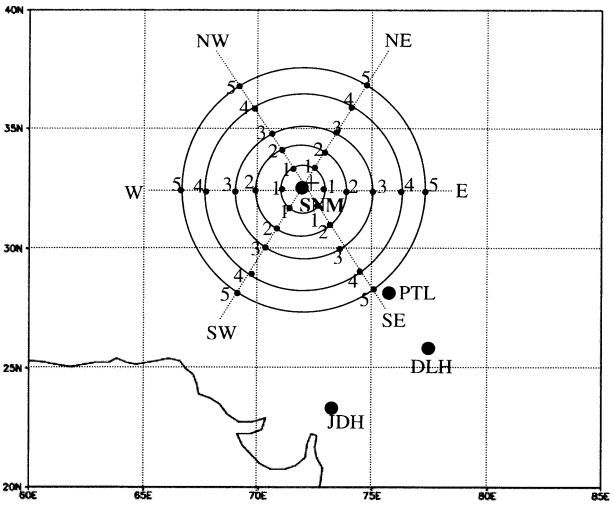

FIG. 3. The location of meteorological stations from which data have been used in this study: PTL, Patiala; DLH, Delhi; JDH, Jodhpur; and SNM, Sonamarg, which is the selected location of the study and is indicated by a plus sign (+). NCEP–NCAR reanalysis data are interpolated at locations numbered from 1 to 5 along various geographical directions and are marked by a shaded circle (●).

The NCEP–NCAR reanalyzed global dataset (Kalnay et al. 1996), along with surface and upper-air data of Patiala, Jodhpur, and Delhi from the India Meteorological Department (IMD), at 0000 and 1200 UTC, are used for the development of the models (Fig. 3). For the development of statistical–dynamical models, initially all possible basic as well as derived meteorological fields/parameters are utilized and are subjected to an objective screening procedure to select the most appropriate predictors. Therefore, initially a total of 3306 predictors, as listed in Table 2, were considered for development of statistical–dynamical models based on the PPM concept. The NCEP–NCAR reanalysis is global with horizontal resolution of 2.5° latitude × 2.5° longitude and 18 vertical pressure levels. For the development of the model equations, geopotential height (gpm); dry-bulb temperature (TT); u and v components of wind; vertical velocity and specific humidity at 850-, 700-, 500-, 300-, and 200-hPa levels from NCEP–NCAR reanalysis fields; and IMD upper-air datasets are utilized. Further, derived parameters are also considered such as vorticity, advection of various meteorological fields, and various meteorological indices (Table 2) etc. In addition, as the grid is coarse, from the topographic and terrain conditions' point of view, the NCEP–NCAR analysis data are interpolated at selected sites and around each site in five concentric circles with increasing radii from 0.5° to 2.5° at an interval of 0.5°. Then six equidistance points on each circle around these sites are selected by starting at the east and proceeding counter-clockwise at 60° intervals, as shown in Fig. 3. Such an interpolation of this coarse-resolution dataset to finer grid points of concentric circles does not reflect much physical significance. However, the use of numerical model output at finer grid points as predictors for the PoP and QPF models plays a very significant role in the incorporation of the mesoscale features. While these predictors do not bring much additional information into

TABLE 2. List of potential predictors and their notations used in the present study. The total number of predictors is 3306.

Predictors and their notations	Stations	Time*	Total
Surface data			
Dry-bulb (TT) and dewpoint (TD) temperature, saturation mixing ratio (SM), relative humidity (rh), and zonal (u) and meridional (υ) components of wind	Delhi, Patiala, Jodhpur	−1200 and 0000 UTC	36
Upper-air data			
Dry-bulb and dewpoint temperature; saturation mixing ratio; relative humidity; zonal and meridional components of wind at 850, 700, 500, 300, and 200 hPa; dry-bulb and potential temperature (θ) differences between different levels from surface to 300 hPa; mean of the relative humidity and saturation mixing ratio between various levels; and derived wind shear terms between various levels	Delhi, Patiala, Jodhpur	−1200 and 0000 UTC	474
Stability indices			
Showalter index (SI), Rackliff's index (RI), Jefferson's modified index (JMI), convective index of REEP (CIR), George index (GI), vertical total index (VTI), Cross total index (CTI), total totals index (TTI), Modified George index (MGI), modified vertical total index (MVTI), modified cross total index (MCTI), modified total totals index (MTTI), potential wet-bulb index (PWBI), lifted index (LI), potential instability index (PII), severe weather threat index (SWTI)	Delhi, Patiala, Jodhpur	−1200 and 0000 UTC	96
NCEP interpolated data			
Geopotential height (gpm), dry-bulb temperature, zonal and meridional components of wind, vertical (w) component of wind, and specific humidity (q) at 850-, 700-, 500-, 300-, and 200-hPa levels	30 stencil points	−1200, 0000, and +1200 UTC	2700
		Total	3306

* In the time column, −1200 and 0000 UTC observations are recorded before forecast issuing time, i.e., 0300 and +1200 UTC observations are after forecast issuing time, i.e., they are numerical analyses.

the development of the PPM prediction equations, it is valuable to have these terms in the equation when applying them to the outputs of the high-resolution mesoscale model. These predictors provide a way of making use of the model forecast distinction on this scale.

Precipitation is treated as a binary predictand for PoP. If measurable precipitation is observed, the binary predictand value is set to 1; if no measurable precipitation is observed, the predictand value is set to 0. The threshold value of precipitation is taken as 0.1 cm, which is the least measurable snow depth. The 24-h accumulated snow depths are found to be highly variable. The precipitation reported on a particular day is the accumulated snow depth in the 24 h ending at the reporting time, that is, 0300 UTC. Snowfall depths are classified into four groups: 0.1–12.0, 12.1–24.0, 24.1–48.0, and ≥48.1 cm. This classification is used for avalanche forecasting in India. But for the rest of this work snow depths are converted into the corresponding water equivalent and then compared with the model's precipitation fields. It may be noted that while converting snow depth into the water equivalent, snow density is taken into consideration by computing the standard volume, density, and mass relation.

The PoP model is initiated at 0300 UTC to generate a forecast for the next 24 h. The QPF model is initiated at the same time only if the PoP model indicates the precipitation occurrence as yes. This gives consistently better results than including zero precipitation as a category in the discriminant procedure of the QPF model.

As 24-hourly accumulated precipitation amounts are observed only at 0300 UTC, the PoP and QPF models are initiated at 0300 UTC to generate a forecast for the next 24 h (day 1 forecast). The predictors at three time levels—0000 UTC, 1200 UTC prior to the initiation time of the forecast (0300 UTC), and future time level 1200 UTC—are utilized for the development of the PoP and QPF models based on PPM.

3. Formulation of the probability of precipitation forecast model

Predictors that explain the maximum variance for 24-h PoP forecasts are selected from the set of potential predictors by using the stepwise regression technique following Draper and Smith (1996). The stepwise procedure requires a stopping criterion for the selection of predictors. In this study, the process of selection of predictors is stopped if the new predictor contributes less than 0.5% to the percentage of variance explained by its inclusion as a predictor in the model. Nine significant predictors are selected and then subjected to the development of the PoP model.

In the development of the PoP model, the value of the predictand, Y, is taken as 1 if precipitation occurs and 0 if it does not. Thus, the value of Y varies from 0 (0%) to 1 (100%). Using this philosophy, the values of Y are recalculated for all observations of the developmental sample. If the reestimated value of Y is greater than 1, it is made equal to 1 and if it is less than 0, it is made equal to 0. The recalculated values of Y are grouped into intervals of 0.1. For each group, the observed probabilities of occurrence and nonoccurrence of precipitation are evaluated. The results for one site,

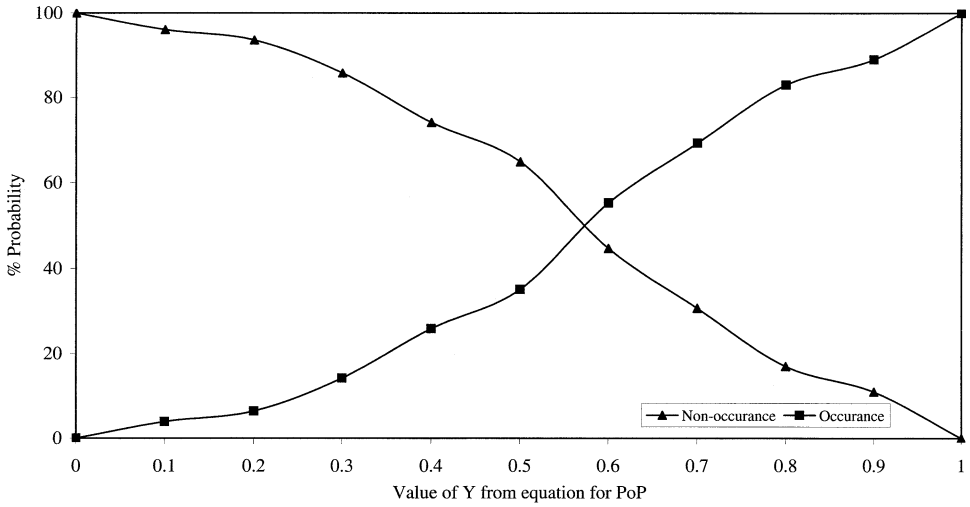

FIG. 4. Reliability diagram for the probability of occurrence–nonoccurrence of precipitation events at Sonamarg using the regression method.

Sonamarg, are presented in the reliability diagram in Fig. 4 for the PoP model along with the best-fit curve. A cutoff point (where curves representing occurrence and nonoccurrence intersect) is chosen between 0 and 1 as given in the reliability diagram (Fig. 4) for Sonamarg. The purpose is to find the threshold value of Y for converting the probability forecast into a categorical forecast of the occurrence or nonoccurrence of precipitation. For Sonamarg, if Y is less than 0.55, nonoccurrence of precipitation is forecast and if Y is greater than or equal to 0.55, occurrence of precipitation is forecast. Similarly the cutoff values for Haddan Taj and Manali are 0.60 and 0.54, respectively. It may be noted that the PoP on the occurrence of precipitation can be predicted as such in terms of a probability percentage. However, as the precipitation is recorded only categorically—that is occurred/not occurred as an amount of precipitation—for the evaluation of the PoP model the probabilistic percentage prediction is converted into a categorical forecast as stated above. Thus, the PoP model can be used either for probabilistic prediction or a categorical forecast.

The predictors that are selected for PoP forecasting are given in Table 3 for Sonamarg, Haddan Taj, and Manali, respectively. Letters and numbers (prefix to the notation of the selected predictor) in the notation of the predictor represent the geographical direction toward which that station is located and the number of the circle in which that predictor belongs, respectively (shown in Fig. 3). The superscript represents the time at which that candidate predictor is observed and the subscript represents the level at which that candidate predictor is observed or levels between which the mean/difference of that candidate predictor is computed. These are interpolated from the NCEP–NCAR reanalysis data. For example, $E3(w)^{00UTC}_{850hPa}$ indicates the vertical component of wind (w) from the NCEP–NCAR reanalysis interpolated at circle point 3 toward the east. The superscript shows that this predictor comes from 0000 UTC, and the subscript shows that it is for 850 hPa. Predictors only having a letter as a prefix to their notation are station data from IMD and that letter is the first letter of that station name. For example, $P(TT)^{00UTC}_{Surface}$ represents the dry-bulb temperature (TT) at the surface that is observed at 0000 UTC at Patiala. The cumulative variance explained, correlation coefficients, and multiple correlation coefficients explained by the selected predictors at three sites are also presented in Table 3.

Vertical velocity at station E3 is negatively correlated to the occurrence of precipitation at all three stations. Rising motion leads to the condensation of the available moisture and hence improves the chances of the occurrence of precipitation. Therefore, this component supports cloud formation and hence precipitation. Further, the surface dry-bulb temperature at Patiala also shows a significant contribution toward the occurrence of precipitation at Sonamarg and Manali. Most of the time, high temperatures and specific humidities at the surface, high values of specific humidity at 500 hPa, and warm air between 500 and 850 hPa are conducive to the occurrence of precipitation. All of the predictors selected for the PoP model have a physical basis for the occurrence of precipitation. The correlation between the occurrence–nonoccurrence of precipitation and its forecast at Sonamarg, Haddan Taj, and Manali are 0.58, 0.55, and 0.43, respectively.

4. Formulation of the quantitative precipitation forecast model

Precipitation at the three selected sites is mainly due to WDs. The amount of precipitation is extensively modulated due to the existing orography. Mesoscale circulation contributes immensely toward defining the type

TABLE 3. Variance explained and correlation coefficient by the selected predictors for forecasting PoP.

Sonamarg			Haddan Taj			Manali		
Predictors*	Cumulative variance explained	Correlation coefficient	Predictors	Cumulative variance explained	Correlation coefficient	Predictors	Cumulative variance explained	Correlation coefficient
$E3(w)^{00UTC}_{850hPa}$	23.9	−0.49	$E3(w)^{00UTC}_{700hPa}$	20.22	−0.45	$E3(w)^{00UTC}_{700hPa}$	10.43	−0.32
$P(TT)^{00UTC}_{Surface}$	28.4	+0.39	$P(TT)^{00UTC-12UTC}_{Surface-700hPa}$	24.26	+0.39	$P(rh)^{00UTC-12UTC}_{700hPa}$	13.35	+0.28
$SW2(TT)^{+12UTC}_{850hPa}$	29.8	−0.02	$NW5(gpm)^{00UTC}_{850hPa}$	25.71	−0.27	$J(TD)^{-12UTC}_{700hPa}$	14.40	−0.05
$E3(q)^{00UTC}_{500hPa}$	30.6	+0.38	$D(u)^{-12UTC}_{Surface}$	27.11	−0.29	$P(rh)^{00UTC}_{(Surface+900hPa+850hPa)/3}$	15.17	+0.25
$P(u)^{00UTC}_{850hPa-500hPa}$	31.4	+0.24	$W5(TT)^{00UTC}_{700hPa}$	27.85	−0.22	$D(u)^{00UTC}_{700hPa}$	15.96	+0.11
$SW2(T)^{-12UTC}_{850hPa}$	31.8	+0.06	$SE4(q)^{00UTC}_{500hPa}$	28.59	+0.25	$NW5(TT)^{00UTC}_{200hPa}$	16.56	−0.11
$P(TT)^{-12UTC}_{Surface-900hPa}$	32.3	−0.11	$D(u)^{-12UTC}_{850hPa-500hPa}$	29.51	−0.18	$J(\theta)^{00UTC}_{Surface-700hPa}$	17.11	−0.04
$SE4(q)^{00UTC}_{500hPa}$	32.7	+0.02	$D(rh)^{-12UTC}_{(Surface+900hPa+850hPa)/3}$	30.19	+0.30	$J(u)^{-12UTC}_{Surface}$	17.81	+0.17
$D(\theta)^{00UTC}_{Surface-900hPa}$	33.2	+0.08	$W5(w)^{-12UTC}_{850hPa}$	30.70	−0.02	$P(u)^{-12UTC}_{700hPa}$	18.26	+0.07
MCC		0.58			0.55			0.43

* Superscript to the predictor indicates time level at which predictors are used. Here −12UTC stands for predictors before start of the forecast issuing time of 0300 UTC, whereas 12UTC stands for predictors obtained 9 h after forecast issuing time by integration of numerical models. Subscript stands for level at which predictor is observed or levels between which means/differences of predictor are computed.

and amount of precipitation. Due to the high spatial and temporal variability of the precipitation, a four-group classification of snow depth is used: 0.1–12.0, 12.1–24.0, 24.1–48.0, and ≥48.1 cm.

Probabilistic QPF models are developed using multiple discriminant analysis (MDA). The MDA procedure yields (G-1) discriminant functions for the G groups, which are used to classify an event (Miller 1962). Klein (1978) and Wilson (1982) have used MDA for forecasting precipitation amounts.

The QPF model is initiated at 0300 UTC only if the PoP model forecasts the occurrence of precipitation. The predictors selected for the PoP model are used in the development of the QPF model. However the QPF model is not constrained by the PoP model as far as the development and functioning of the QPF model is concerned. The QPF model provides the probabilistic forecast of the most likely group in terms of precipitation during the next 24 h. Since there are four groups in the present study, the MDA procedure yielded three discriminant functions of the form

$$z_g = w_1x_1 + w_2x_2 + w_3x_3 + \cdots + w_mx_m, \qquad (1)$$

where z_g are discriminant scores (functions), w_i are the discriminant weights (coefficients), and x_i are the independent variables. The interpretation of the discriminant weights involves the examination of the sign and the magnitude of the weights. Independent variables with relatively large weights contribute more to the discriminating power of the function than the smaller ones. Thus, when the sign is ignored, each weight represents the relative contribution of its associated variable to that discriminant function. The sign merely denotes that the variables make either a positive or a negative contribution. The models are evaluated using developmental data as well as test datasets.

A set of observations (e.g., the nine predictors) is assigned to one of the four groups using the sum of the squared distance principle. That is, an observation y is assigned to group g if

$$\sum_{m=1}^{M} [d_m(y - \overline{x}_g)]^2 \leq \sum_{m=1}^{M} [d_m(y - \overline{x}_h)]^2, \quad \text{for all } h \neq g, \qquad (2)$$

where d_m are the discriminant functions (in our case $M = 3$), y is the set of observations of the predictors (x_1, . . . , x_9), and x_g is the vector of mean values of the predictor variables in the four groups.

5. Experiments for the validation of the PoP and QPF models

The PoP and QPF models are evaluated with independent DJFM data for 1996–97. Four experiments are designed to evaluate the performance of the models with four different types of independent datasets as predictors. Predictors selected by the models from station data,

namely, Jodhpur, Patiala, and Delhi, are the same in all four of the experiments. The rest of the predictors, selected from the reanalysis data and numerical model output, are interpolated at 30 stencil points (Fig. 3) as mentioned in section 2. These experiments are formulated to compare the performance of the PoP and QPF models based on the concept of PPM using selected predictors from different types of analyses and model outputs.

a. Experiment 1 (Ex-1)

In experiment 1, IMD station observations and NCEP–NCAR reanalysis data for December 1996 and January, February, and March 1997 (DJFM 1996–97) are used as predictors. The NCEP–NCAR reanalysis data are available at a horizontal resolution of 2.5° latitude × 2.5° longitude. The NCEP–NCAR reanalyses are interpolated at 30 stencil points (Fig. 3) to provide the required predictors for evaluating the performance of the PoP and QPF models with independent datasets. It may be noted that as the PoP and QPF models were developed on the concept of the PPM, some of the predictors at future time steps are required. Therefore, experiment Ex-1 with the NCEP–NCAR reanalysis data as predictors is hypothetical from an operational point of view. However, it is an appropriate experiment with 1996–97 analyses as independent cases for evaluation as well as a comparison of the performance of the PoP and QPF models.

b. Experiment 2 (Ex-2)

In method 2, the PoP and QPF model predictors are obtained from the NCMRWF operational analysis data for DJFM 1996–97 and IMD station observations. The NCMRWF operational analysis is available at a horizontal resolution of 1.5° latitude × 1.5° longitude. The NCMRWF analysis is interpolated at 30 stencil points (Fig. 3) to provide the required predictors to evaluate the performance of the PoP and QPF models with independent datasets. Like Ex-1, this is also a hypothetical experiment from an operational point of view.

c. Experiment 3 (Ex-3)

In experiment 3 (Ex-3), IMD observations and the NCMRWF operational global spectral model T80 day 1 model forecast are used as predictors to evaluate the performance of the PoP and QPF models for DJFM 1996–97. Details of the T80 spectral global model are given in the work of Mohanty et al. (1994). The T80 model outputs are available at a horizontal resolution of 1.5° latitude × 1.5° longitude and are interpolated at 30 stencil points (Fig. 3) to provide the required predictors. This is a realistic experiment as the future state of atmospheric circulations is taken from the T80 numerical model output for the PoP and QPF models based on the PPM concept and thus can be used in real-time operational applications.

TABLE 4. MM5 model configuration used in this study.

Model	Fifth-generation PSU–NCAR Mesoscale Model, version 2.12
Dynamics	Nonhydrostatic with 3D Coriolis force
Main prognostic variables	U, v, w, T, p', and q
Map projection	Lambert conformal mapping
Central point of domain	33°N, 75°E
No. of horizontal grid points	165 and 105 grid points for x and y, respectively
Horizontal grid distance	60 km
No. of vertical levels	23 half sigma levels (7 levels within boundary layer) (24 full sigma levels are 1, 0.99, 0.98, 0.96, 0.93, 0.89, 0.85, 0.8, 0.75, 0.7, 0.65, 0.6, 0.55, 0.5, 0.45, 0.4, 0.35, 0.3, 0.25, 0.2, 0.15, 0.1, 0.05, and 0.0)
Horizontal grid scheme	Arakawa B grid
Time integration scheme	Leapfrog scheme with time-splitting technique
Lateral boundary conditions	Nudging toward the NCEP–NCAR reanalysis
Radiation scheme	Dudhia's shortwave/longwave simple cloud radiation scheme with frequency of 30 min
Planetary boundary layer parameterization schemes	Hong–Pan (as implemented in NCEP MRF model)
Cumulus parameterization schemes	Betts–Miller
Microphysics	Explicit scheme of Reisner (mixed phase)
Soil model	Multilayer soil model
Topography	U.S. Geological Survey 10′ topography
SST and surface parameters	NCEP–NCAR reanalysis

d. Experiment 4 (Ex-4)

The fourth experiment (Ex-4) uses numerical model output from the fifth-generation Pennsylvania State University–NCAR (PSU–NCAR) Mesoscale Model (MM5) for DJFM 1996–97. In this method, observations from IMD stations and the day 1 forecast from the mesoscale model provide potential predictors. The MM5 simulations use the initial and boundary conditions from the NCEP–NCAR reanalysis data. Details of the MM5 are given by Dudhia et al. (1998). A brief description of the model configuration is presented in Table 4. The MM5 outputs have a horizontal resolution of 0.5° latitude × 0.5° longitude. Here, too, the MM5 day 1 forecast model outputs are interpolated at 30 stencil points (Fig. 3) to serve as potential predictors. It may be noted that in this case the model output data used as predictors over the data-sparse region are of the same horizontal resolution as that of the concentric circles with 30 stencil points (Fig. 3). Thus the mesoscale features simulated

by the high-resolution MM5 over the western Himalayas are preserved without any horizontal smoothing in the process of interpolation to an equivalent resolution, 30 stencil points (Fig. 3), to provide potential predictors for the PoP and QPF models. It may be noted that this type of experiment is close to a real-time operational setup, provided the MM5 uses global simulation fields as lateral boundary conditions.

In addition to these four sets of numerical experiments for estimating and evaluating the PoP and QPF models, direct numerical model output from the T80 global spectral model (T80D1) and the MM5 regional mesoscale model (MM5D1) are also examined. Thus, a total of six sets of predictions of PoP and QPF are produced for the comparison and evaluation of the performance of various models.

6. Results and discussion

The results of the PoP and QPF models determined with the dependent/developmental datasets from DJFM 1984–96 and independent datasets from DJFM 1996–97 are presented. The performances of the PoP and QPF models are evaluated by computing various statistical skill scores. The verification of categorical forecasts and the percentage of correct forecasts are also computed. Comprehensive analyses are carried out to assess the model skills of the four experiments and the two direct NWP model outputs. Out of the six sets of forecasts for the independent cases during DJFM 1996–97, Ex-1 and Ex-2 may be considered to be control experiments, as selected predictors are taken from the future state of the analysis sets, which would not be available for operational/real-time forecasts. These control experiments will not only be idealized cases for comparison and evaluation of the PoP and QPF models with different sets of predictors, but can also be used to understand the objective forecast approach over a data-sparse region with rugged orography.

In this section, emphasis has been given to the performance of PoP and QPF models based on the PPM concept using independent datasets for DJFM 1996–97. However, for the sake of completeness, the performance of these models with development datasets from DJFM 1984–96 is also presented. The performance of the models is examined for all three of the locations viz, Sonamarg, Haddan Taj, and Manali, which represent different geographical regions over the western Himalayas.

a. Performance of the PoP forecast model

The regression model for forecasting PoP at these sites is evaluated using the developmental DJFM data for the 12-yr period 1984–96 and the independent data for DJFM 1996–97. For the purpose of verification of the categorical forecasts, a 2×2 contingency table is prepared and the verification parameters and skill scores are evaluated as defined in appendix A (Wilks 1995).

For the developmental data, Table 5 illustrates that the probability of detection (POD) of the occurrence of precipitation at Sonamarg and Haddan Taj is relatively higher than that at Manali. The false alarm rate (FAR) for all three locations does not exceed 0.13, which illustrates that the PoP has a better POD of the nonoccurrence (C-NON) of precipitation (POD in the range of 0.94–0.97) than it does the occurrence of precipitation (POD ranging from 0.68 to 0.86). This may be attributed to the fact that the number of no precipitation days is generally higher compared to the number of days with precipitation. The Heidke skill score (HSS) is 0.8 for Sonamarg and Haddan Taj, while it is 0.7 for Manali. The other skill scores/evaluation indices for the model with the dependent dataset also show reasonably high values toward the perfect forecast criteria (appendix A). It is interesting to note that the overall performance of the PoP model, which is measured by the percent correct (PC), is very high and is about 90% at all three locations. All the forecast verification indices estimated from the contingency tables clearly demonstrate that the PoP model at all three locations provides very satisfactory performance regard to with the developmental data.

The performance of the PoP models with the independent dataset from DJFM 1996–97 is investigated extensively using different types of predictors in Ex-1–Ex-4 and is also compared with direct numerical model output, T80D1 and MM5D1. The comparison of Ex-1 and Ex-2, which are the control experiments with the NCEP–NCAR and NCMRWF analyses as predictors, indicates that, as with the dependent cases, the skill of the model in predicting the nonoccurrence events more successfully with correct nonoccurrence (C-NON) is higher than the probability of detection (POD). The FAR in both of the control run experiments does not exceed 0.37. In Ex-1 and Ex-2, the HSSs at Sonamarg and Haddan Taj are about 0.6 except at Manali in Ex-2 where the NCMRWF analysis provides the predictors. The overall performances of both of the control experiments as illustrated by percent correct are quite satisfactory, within the range of 81%–88%.

The performance of the models with independent data as illustrated in Ex-3 and Ex-4 depicts that the PoP models can predict the nonoccurrence of precipitation events better than it can the occurrence of precipitation events. This aspect of the PoP models agrees with the dependent data as well as the control experiments. Similarly, the performance of the PoP at Sonamarg and Haddan Taj with respect to POD is reasonably higher than that at Manali. The Heidke skill scores for Ex-3 and Ex-4 are almost in the same range as those of the control experiments. The overall performance of Ex-3 and Ex-4 with respect to percent correctness is almost the same for all three stations. In Table 5, the percent correct with these two experiments ranges from 85% to 89%, which is slightly better than that of the control experiments. However, the total number of occurrences

TABLE 5. Verification measures for the PoP model. Ex-1 uses NCEP–NCAR reanalysis, Ex-2 uses NCMRWF analysis, Ex-3 uses T80 global spectral model outputs, and Ex-4 uses MM5 regional model outputs.

		Independent data (DJFM 1996–97)					
		Based on PPM				Direct model output	
Measure	Dependent data (DJFM 1984–96)	Ex-1	Ex-2	Ex-3	Ex-4	T80D1	MM5D1
Sonamarg							
POD	0.86	0.71	0.61	0.68	0.74	0.61	0.39
FAR	0.07	0.16	0.21	0.16	0.18	0.63	0.35
MR	0.14	0.29	0.39	0.32	0.26	0.39	0.61
C-NON	0.95	0.94	0.93	0.94	0.93	0.53	0.90
CSI	0.80	0.63	0.52	0.60	0.64	0.30	0.33
TSS	0.81	0.65	0.53	0.62	0.66	0.14	0.30
HSS	0.81	0.68	0.57	0.66	0.68	0.12	0.33
BIAS	0.92	0.84	0.76	0.82	0.89	1.63	0.61
PC	91	87	83	86	87	55	74
Haddan Taj							
POD	0.86	0.71	0.82	0.82	0.84	0.58	0.47
FAR	0.08	0.23	0.21	0.18	0.18	0.63	0.36
MR	0.14	0.29	0.18	0.18	0.16	0.42	0.53
C-NON	0.94	0.90	0.90	0.92	0.92	0.55	0.88
CSI	0.80	0.59	0.67	0.69	0.71	0.29	0.38
TSS	0.80	0.61	0.72	0.73	0.76	0.13	0.35
HSS	0.80	0.63	0.71	0.73	0.75	0.12	0.38
BIAS	0.94	0.92	1.03	1.00	1.03	1.55	0.74
PC	90	84	88	88	89	56	75
Manali							
POD	0.68	0.64	0.43	0.50	0.57	0.61	0.71
FAR	0.13	0.28	0.37	0.22	0.16	0.65	0.55
MR	0.32	0.36	0.57	0.50	0.43	0.39	0.29
C-NON	0.97	0.92	0.92	0.96	0.97	0.66	0.74
CSI	0.60	0.51	0.34	0.44	0.52	0.28	0.38
TSS	0.63	0.57	0.35	0.46	0.54	0.26	0.46
HSS	0.70	0.59	0.40	0.52	0.61	0.21	0.38
BIAS	0.77	0.89	0.68	0.64	0.68	1.75	1.57
PC	90	86	81	85	88	64	74

of precipitation events with the independent data from DJFM 1996–97 is limited to about 35 cases.

The direct numerical model output experiment MM5D1 illustrates that the numerical models also predict the nonoccurrence of precipitation events better than the probability of precipitation events. The numerical models give larger FARs compared to the statistical dynamical PoP model. The overall performance of MM5 is better than that of the T80 spectral global model. The MM5 also has a better percent correct score than does the global spectral T80 model. Comparison of all the statistical verification parameters/skill scores clearly indicates that the overall performance of the MM5 is better than that of the global spectral T80 model. This may be attributed to the fact that the mesoscale model is of higher resolution at 0.5° latitude × 0.5° longitude and can resolve the complex topography more accurately than the T80 model, having a horizontal resolution of 1.5° latitude × 1.5° longitude.

It is interesting to compare the performance of the numerical models T80D1 and MM5D1 with the corresponding statistical dynamical models Ex-3 and Ex-4 for PoP based on these numerical model outputs. With respect to all the evaluation parameters/skill scores, Ex-3 and Ex-4 yielded considerably better results than the corresponding direct numerical model outputs except for POD at Manali. The result with the most contrast is that the FAR is considerably reduced by the statistical–dynamical models (Ex-3 and Ex-4) compared to the direct numerical model outputs. The HSS for these statistical–dynamical models is much higher than the HSS for the direct numerical models. Similarly the percent correct with respect to Ex-3 and Ex-4 is higher than for the respective numerical model outputs. These results clearly demonstrate that the use of numerical model outputs as predictors in statistical–dynamical models based on the PPM concept considerably improves the performance of location-specific PoP as compared to the direct numerical model outputs.

b. Performance of the QPF model

QPF models based on discriminant analysis to predict the categorical quantity of precipitation are evaluated with the development and independent datasets. The skill scores and the other verification measures are calculated using a 4 × 4 contingency table (appendix B; Wilks 1995). The skill scores and other verification mea-

TABLE 6. Contingency table and skill scores of the QPF model. Ex-1 uses NCEP–NCAR reanalysis, Ex-2 used NCMRWF analysis, Ex-3 uses T80 global spectral model outputs, and Ex-4 uses MM5 regional model outputs.

Categories	Measure	Dependent data (DJFM 1984–96)	Independent data (DJFM 1996–97)					
			Ex-1	Ex-2	Ex-3	Ex-4	T80D1	MM5D1
Sonamarg								
I	CSI	0.47	0.76	0.91	0.76	0.72	0.46	0.30
II	CSI	0.25	0.00	0.40	0.57	0.00	0.31	0.20
III	CSI	0.18	0.33	0.50	0.50	0.80	0.00	0.30
IV	CSI	0.26	0.67	1.00	0.25	1.00	0.00	0.30
	HSS	0.22	0.49	0.68	0.68	0.77	0.14	0.26
	PC	45.0	74.0	78.0	81.0	85.0	43.0	47.0
Haddan Taj								
I	CSI	0.40	0.34	0.53	0.44	0.55	0.40	0.36
II	CSI	0.16	0.23	0.45	0.30	0.25	0.22	0.14
III	CSI	0.21	0.00	0.00	0.25	0.16	0.20	0.00
IV	CSI	0.18	0.16	0.22	0.22	0.22	0.20	0.00
	HSS	0.19	0.12	0.33	0.28	0.30	0.25	0.05
	PC	43.0	41.0	52.0	48.0	53.0	45.0	28.0
Manali								
I	CSI	0.38	0.50	0.50	0.57	0.67	0.44	0.40
II	CSI	0.20	0.43	0.30	0.60	0.40	0.22	0.09
III	CSI	0.15	0.00	0.00	0.40	0.50	0.20	0.67
IV	CSI	0.17	0.40	0.50	0.00	0.30	0.00	0.13
	HSS	0.18	0.37	0.33	0.49	0.54	0.17	0.17
	PC	41.0	56.0	58.0	64.0	69.0	41.0	40.0

sures of the QPF models are illustrated in Table 6 for Sonamarg, Haddan Taj, and Manali.

For the developmental data, the critical success index (CSI) for the QPF model is higher in category I as compared to other categories at all three stations. This illustrates the fact that the QPF model can predict the precipitation amount in lower snowfall categories better than in higher categories. In most of the categories, the CSI is higher at Sonamarg than at Haddan Taj and Manali. The HSS ranges from 0.18 to 0.22 at these sites. It is interesting to note that the overall performance of the QPF model in terms of percent correct (PC) with the developmental sample ranges from 41% to 45%. All the forecasts estimated from the contingency tables show that the QPF models at all three locations are able to provide reasonable performance over these data-sparse regions.

The performance of the QPF models with the independent data from DJFM 1996–97 is evaluated using different types of predictors in Ex-1–Ex-4 and is compared with direct numerical model outputs. Experiments Ex-1 and Ex-2 are control model runs with the NCEP–NCAR and NCMRWF operational analyses, respectively. Higher CSI values are shown for Ex-2 than for Ex-1. This illustrates the fact that Ex-2 produces a better prediction of the probability of occurrence of the quantity of precipitation in respective categories than does Ex-1 at Sonamarg and Haddan Taj. These two experiments show very similar results at Manali, but the overall performance of Ex-2 is better. At Sonamarg and Haddan Taj, the HSSs are reasonably higher in Ex-2 (0.68 and 0.33) than in Ex-1 (0.49 and 0.12), whereas the reverse is true at Manali (0.33 for Ex-2 and 0.37 for Ex-1). The overall percent correct for Ex-1 and Ex-2 are 74% and 78% at Sonamarg, 41% and 52% at Haddan Taj, and 56% and 58% at Manali.

At Sonamarg, a comparison of the CSI of the QPF models with independent data in Ex-3 and Ex-4 indicates that Ex-4 better predicts the higher categories of precipitation than does Ex-3, whereas Ex-3 performs better in the lower categories of precipitation. However, at Haddan Taj and Manali Ex-4 performs better in the lower categories than the higher categories. At all three locations the Heidke skill scores are better for Ex-4 than for Ex-3. The percent correct with these two experiments range from 0.28 to 0.77 and are better than are those of the control experiments (Ex-1 and Ex-2). Further, at all three locations, the overall performance of Ex-4 is better than Ex-3.

The direct numerical model output experiments T80D1 and MM5D1 demonstrate that the CSI is higher for category I than for the other categories except that the CSI is 0.67 for category III at Manali, suggesting that value is a fluke. The overall performance of both the numerical model outputs are almost the same at Manali (41% and 40%), whereas at Haddan Taj, the T80D1 model performs better with 45% versus 28% percent correct and at Sonamarg, the MM5D1 model performs better with 47% versus 43% percent correct. However, it may be noted that out of 35 cases with precipitation, the lowest category of snow depth is the most common. In the highest category, the number of events does not exceed 5. Therefore, the results of the

QPF model for the highest category of precipitation may be considered to be tentative.

It is of interest to compare the performance of numerical models T80D1 and MM5D1 with the corresponding statistical dynamical model results of Ex-3 and Ex-4 based on these numerical model outputs. The overall values of the CSI, HSS, and PC are reasonably higher for the statistical dynamical models (Ex-3 and Ex-4) as compared to direct numerical model outputs. These results again confirm the fact that the use of large-scale meteorological fields of numerical model outputs as predictors in statistical–dynamical models significantly improves the performance of the QPF models as compared to direct numerical model outputs.

7. Conclusions

PoP and QPF models are developed and their performances are evaluated with four experiments and two direct numerical model outputs. Based on the evaluation of the performance of the models, the following broad conclusions are drawn.

The PoP models provide satisfactory results in forecasting the probabilistic occurrence–nonoccurrence of precipitation. It may be noted that the nonoccurrence of precipitation is better predicted by PoP models than is the occurrence of precipitation. The statistical–dynamical models for forecasting QPF by classification of precipitation amounts into four categories perform with reasonable accuracy. Further, PoP models perform considerably better than the QPF models based on CSI, HSS, and PC skill scores. This may be attributed to the fact that precipitation amounts are highly variable in space and time as compared to the occurrence of precipitation, which is mainly due to the passage of large-scale synoptic events during winter months.

A numerical model with finer resolution can provide better representation of the rugged topography over the region of interest and hence the MM5 model simulates weather events better than the coarser-resolution global T80 model. The use of numerical weather prediction model outputs as predictors in statistical–dynamical models substantially improves the forecast of the probability of occurrence of precipitation as well as the amount of precipitation as compared to direct numerical model outputs. Further, the MM5 model outputs as predictors in a statistical–dynamical model (Ex-4) outperform T80 model outputs as predictors in a statistical–dynamical model (Ex-3).

From this study, it may be concluded that numerical model outputs used as predictors in a statistical–dynamical model improve PoP and QPF forecasts over a data-sparse mountain region like the western Himalayas. Further, the improvement in the prediction of precipitation will depend on the improvement in the performance of mesoscale models along with an enhanced mesoscale observational network, mesoscale data assimilation, and better use of nonconventional data from various sources.

Acknowledgments. The authors acknowledge the Snow and Avalanche Study Establishment (SASE), Chandigarh, India, for providing valuable datasets over the western Himalayas and continuous support in various ways to help accomplish this work. The authors acknowledge the India Meteorological Department (IMD); the National Center for Medium Range Weather Forecasting (NCMRWF), New Delhi, India; and the U.S. National Centers for Environmental Prediction (NCEP) for providing valuable datasets for accomplishing this work. The authors are grateful to all three anonymous referees for their valuable and constructive comments, which helped to improve the quality of this work.

APPENDIX A

Verification Measures Used for Forecast Evaluation

The values in Table A1 are defined as follows:

1) When an event is predicted to occur (forecast occurrence) and in reality it does occur (observed occurrence), then it is classified as A; otherwise (observed nonoccurrence) it is classified as C;
2) when an event is predicted not to occur (forecast nonoccurrence) and in reality it does occur (observed occurrence), then it is classified as B; otherwise (observed nonoccurrence) it is classified as D;
3) A + B is the total number of cases of occurrence of precipitation as observed;
4) C + D is the total number of cases of nonoccurrence of precipitation as observed; and
5) A + B + C + D is the total number of forecasts.
6) Evaluation measures derived from Table A1 are

Probability of detection (POD)

$$\text{POD} = \frac{\text{A}}{\text{A} + \text{B}},$$

False alarm rate (FAR)

$$\text{FAR} = \frac{\text{C}}{\text{C} + \text{A}},$$

Miss rate (MR)

$$\text{MR} = \frac{\text{B}}{\text{B} + \text{A}},$$

Correct nonoccurrence (C-NON)

$$\text{C-NON} = \frac{\text{D}}{\text{D} + \text{C}},$$

Critical success index (CSI)

TABLE A1. The 2 × 2 contingency table format.

	Forecast	
Observed	Yes	No
Yes	A	B
No	C	D

$$\mathrm{CSI} = \frac{A}{A + B + C},$$

True skill score (TSS)

$$\mathrm{TSS} = \frac{A}{A + B} + \frac{D}{D + C} - 1,$$

Heidke skill score (HSS)

$$\mathrm{HSS} = \frac{2(AD - BC)}{B^2 + C^2 + 2AD + (B + C)(A + D)},$$

Bias (BIAS) for occurrence

$$\mathrm{BIAS} = \frac{A + C}{A + B}, \text{ and}$$

Percentage correct (PC)

$$\mathrm{PC} = \frac{A + D}{A + B + C + D}100\%.$$

For a best/perfect forecast series, $B = 0$ and $C = 0$ and hence

$\mathrm{POD} = 1$, $\mathrm{FAR} = 0$, $\mathrm{MR} = 0$, $\text{C-NON} = 0$, $\mathrm{Bias} = 1$, $\mathrm{CSI} = 1$, $\mathrm{TSS} = 1$, $\mathrm{HSS} = 1$, and $\mathrm{PC} = 100\%$.

APPENDIX B

Categorical Verification of Forecasts (Four-Category Events)

In Table B1 the total number of observed events in category I is

$$J = a + b + c + d,$$

the total number of forecast events in category I is

$$N = a + e + i + m, \text{ and}$$

in a similar fashion O, K, P, L, Q, and M are computed. Then the total numbers of events are

$$T = J + K + L + M = N + O + P + Q.$$

Evaluation measures derived from Table B1 are

Percentage correct (PC)

$$\mathrm{PC} = \frac{a + f + k + p}{T}100\%,$$

Critical success index (CSI)

$$\mathrm{CSI} = \frac{a}{J + N - a}, \quad \frac{f}{K + O - f}, \quad \frac{k}{L + P - k}, \quad \frac{p}{M + Q - p},$$

Heidke skill score (HSS)

$$\mathrm{HSS} = \frac{a + f + k + p - \dfrac{JN + KO + LP + MQ}{T}}{T - \dfrac{JN + KO + LP + NQ}{T}}.$$

TABLE B1. The 4 × 4 contingency table format.

	Forecast				
Observed	I	II	III	IV	Total
I	a	b	c	d	J
II	e	f	g	h	K
III	i	j	k	l	L
IV	m	n	o	p	M
Total	N	O	P	Q	T

REFERENCES

Carter, G. M., 1986: Moving towards a more responsive statistical guidance system. Preprints, *11th Conf. on Weather Analysis and Forecasting*, Kansas City, MO, Amer. Meteor. Soc., 39–45.

——, P. J. Dallavalle, and H. R. Glahn, 1989: Statistical forecasts based on the National Meteorological Center's weather prediction system. *Wea. Forecasting*, **4,** 401–412.

Draper, N. R., and H. Smith, 1966: *Applied Regression Analysis.* Wiley and Sons, 407 pp.

Dudhia, J., D. Gill, Y. R. Go, D. Hansen, and K. Manning, cited 1998: PSU/NCAR mesoscale modeling system tutorial class notes and user's guide: MM5 modeling system version 2. [Available online at http://www.mmm.ucar.edu/mm5/doc.html.]

Glahn, H. R., and D. A. Lowry, 1969: An operational method for objectively forecasting probability of precipitation. ESSA Tech. Memo. WBTM 27, 24 pp.

——, and ——, 1972: The use of model output statistics (MOS) in objective weather forecasting. *J. Appl. Meteor.*, **11,** 1203–1211.

Kalnay, E., and Coauthors, 1996: The NCEP/NCAR 40-Year Reanalysis Project. *Bull. Amer. Meteor. Soc.*, **77,** 437–471.

Klein, W. H., 1978: Objective forecasts of local weather by means of model output statistics. *Proc. ECMWF Seminar on the Interpretation and Use of Large-Scale Numerical Forecast Products*, Reading, United Kingdom, European Centre for Medium-Range Weather Forecasts, 186–220.

——, B. M. Lewis, and I. Enger, 1959: Objective prediction of 5-day mean temperature during winter. *J. Meteor.*, **16,** 672–682.

Kriplani, R. H., and S. V. Singh, 1986: Rainfall probabilities and amounts associated with monsoon depressions over India. *Mausam*, **37,** 111–116.

Kruizinga, S., 1982: Statistical interpretation of ECMWF products in Dutch weather service. *Proc. 1982 Seminar/Workshop on Interpretation of NWP Products*, Reading, United Kingdom, European Centre for Medium-Range Weather Forecasts, 347–364.

Kumar, A., and L. C. Ram, 1995: Semi-quantitative forecasts for Rapti catchment by synoptic analogue method. *Mausam*, **46,** 97–99.

Maini, P., A. Kumar, S. V. Singh, and L. S. Rathore, 2002: Statistical interpretation of NWP products in India. *Meteor. Appl.*, **9,** 21–31.

Miller, R. G., 1962: *Statistical Prediction by Discriminant Analysis. Meteor. Monogr.*, No. 25., Amer. Meteor. Soc., 3–14.

Mohanty, U. C., G. R. Iyenger, S. Basu, E. Klinker, G. H. Shite, S. F. Milton, and D. Singh, 1994: An intercomparision of medium range prediction of selected features of Asian summer monsoon activity with operational GCMs. *Proc. Int. Conf. on Monsoon Variability and Prediction*, Geneva, Switzerland, WMO Tech. Doc. 619, 351–361.

——, N. Ravi, and O. P. Madan, 2001: Forecasting precipitation over

Delhi during the southwest monsoon season. *Meteor. Appl.,* **8,** 11–21.
Paegle, J. N., 1974: Prediction of precipitation probability based on 500 mb flow types. *J. Appl. Meteor.,* **13,** 213–220.
Upadhyay, D. S., N. Y. Apte, S. Kaur, and S. P. Singh, 1986: A dynamical approach to quantitative precipitation forecast. *Mausam,* **37,** 369–372.
Wilks, D. S., 1995: *Statistical Methods in the Atmospheric Sciences.* Academic Press, 466 pp.
Wilson, L. J., 1982: Weather element prediction by discriminant analysis. *Proc. 1982 Seminar/Workshop on Interpretation of NWP Products,* Reading, United Kingdom, European Centre for Medium-Range Weather Forecasts, 311–346.